The IMMUNE-ASSOCIATED NUCLEOTIDE-BINDING 9 protein is a regulator of basal immunity in *Arabidopsis thaliana*

Yuanzheng Wang[1,2], Tabata Rosas-Diaz[1], Carlos Caceres-Moreno[1,2], Rosa Lozano-Duran[1] and Alberto P. Macho[1,*].

[1]Shanghai Center for Plant Stress Biology, CAS Center for Excellence in Molecular Plant Sciences; Shanghai Institutes of Biological Sciences, Chinese Academy of Sciences, Shanghai 201602, China.
[2]University of Chinese Academy of Sciences, Beijing, China.

Running title: IAN9 is a regulator of plant basal immunity

Highlight: IAN9 and its interactor IAP1 act as negative regulators of basal immunity against bacterial pathogens in *Arabidopsis thaliana*.

* Corresponding author: Alberto P. Macho,
alberto.macho@sibs.ac.cn; (+86) 02157078280

Submission date: March 6th 2018

Word count: 5956

Figures: 6 (2 in colour in print)
Supporting figures: 19
Supporting tables: 3

Abstract

A robust regulation of plant immune responses requires multitude of positive and negative regulators that act in concert. The immune-associated nucleotide-binding (IAN) gene family members are associated with immunity in different organisms, although no characterization of their function has been carried out to date in plants. In this work, we analyzed the expression patterns of *IAN* genes and found that *IAN9* is repressed upon pathogen infection or treatment with immune elicitors. *IAN9* encodes a plasma membrane-localized protein that genetically behaves as a negative regulator of immunity. A novel *ian9* mutant generated by CRISPR/Cas9 shows increased resistance to *Pseudomonas syringae*, while transgenic plants overexpressing *IAN9* show a slight increase in susceptibility. *In vivo* immunoprecipitation of IAN9-GFP followed by mass spectrometry analysis revealed that IAN9 associates with a previously uncharacterized C3HC4-type RING finger domain-containing protein that we named IAP1, for IAN9-associated protein 1, which also acts as a negative regulator of basal immunity. Interestingly, neither *ian9* or *iap1* mutant plants show any obvious developmental phenotype, suggesting that they display enhanced inducible immunity rather than constitutive immune responses. Since both *IAN9* and *IAP1* have orthologs in important crop species, they could be suitable targets to generate plants more resistant to diseases caused by bacterial pathogens without yield penalty.

Keywords: Arabidopsis, CRISPR/Cas9, IAN, plant disease, plant immunity, negative regulation, protein complex, *Pseudomonas syringae*.

Introduction

The plant immune system comprises an intricate network of receptors and regulators aimed at keeping the cellular homeostasis in the absence of pathogen threat and responding rapidly to biotic stimuli in order to prevent infection. Plants have evolved to perceive pathogen-derived molecules that constitute signals of a potential invasion, also called invasion patterns (Cook et al, 2015). Conserved microbial molecules constitute good targets for recognition by plants; some of these molecules have been shown to be perceived by plant cells as pathogen-associated molecular patterns (PAMPs; Boller and Felix, 2009). PAMPs are perceived at the cell surface by transmembrane pattern-recognition receptors (PRRs; Zipfel, 2014). PRRs act in coordination with several regulators and additional proteins that mediate signal transduction (Couto and Zipfel, 2016), including mitogen-activated protein kinases (MAPKs), calcium-dependent protein kinases (CDPKs), receptor-like cytoplasmic kinases (RLCKs), and respiratory burst oxidase homologs (RBOHs) (Macho and Zipfel, 2014; Bigeard et al, 2015). Downstream responses include the production of the phytohormone salicylic acid and antimicrobial compounds, the deposition of callose at the cell wall, and extensive transcriptional reprogramming (Boller and Felix, 2009). The activation of immunity is aimed at preventing the proliferation of the perceived pathogen, and prepares plant cells to mount an efficient defence response against subsequent biotic threats. However, defence is costly, in terms of energy investment and the concomitant disruption to the normal developmental program (Huot et al, 2014; Stael et al, 2015), and as such needs to be tightly regulated. For this reason, immune responses are inducible, and negative regulators ensure a firm control of their activated state. On the other hand, it has been demonstrated that activation of defence and inhibition of growth can be uncoupled, so that active defence and growth can occur simultaneously, indicating that developmental alterations are the consequence of an active process, and not necessarily of limiting resources (De Wit et al, 2013; Campos et al, 2016; Scheres and van der Putten, 2017).

Pathogens have developed strategies to manipulate plant cells in order to proliferate inside plant tissues. These include the suppression of plant immunity, the alteration of the physical environment, and the acquisition of nutrients to support pathogenic lifestyle (Win et al, 2012). In Gram-negative bacterial pathogens, the most important virulence factor is the type-III secretion system (T3SS), which injects effector proteins directly inside plant cells (type-III-secreted effectors, T3Es). The manipulation of

plant cellular functions by T3Es is essential for bacteria to proliferate and is required for the development of disease (Macho and Zipfel, 2015; Macho, 2016). However, some plants have evolved intracellular receptors that can perceive T3E activities as an indication of pathogen invasion, hence becoming resistant to bacterial infection. These receptors contain nucleotide-binding and leucine-rich repeat domains (NLRs; Khan et al, 2016). NLR activation contributes to the development of defence responses similar to those established after PRR activation, but are often more intense, and sometimes lead to local cell death, which prevents further pathogen proliferation and spread (Chiang and Coaker, 2015). Both PRRs and NLRs constitute the basis of plant innate immunity, and are the major determinants of basal immunity in plants.

Guanosine triphosphate (GTP)-binding proteins are regulators of various biological processes in eukaryotic cells, such as such as signal transduction, cell proliferation, cytoskeletal organization, and intracellular membrane trafficking, and are classified into numerous families (Takai et al, 2001; Vernoud et al, 2003). IMMUNE-ASSOCIATED NUCLEOTIDE-BINDING/GTPases OF IMMUNITY-ASSOCIATED PROTEINS (IAN/GIMAP) proteins comprise a sub-family of GTPase-like proteins that has been found in anthozoans, vertebrates, and angiosperm plants (Nitta and Takahama, 2007; Weiss et al, 2013). In vertebrates, proteins from the IAN/GIMAP family regulate the development and homeostasis of T cells and are associated to autoimmunity (Nitta and Takahama, 2007). The transcriptional regulation of genes encoding IAN/GIMAP proteins has been linked to immunity in different organisms: in mice, *IAN/GIMAP* genes are mostly expressed in immune tissues (Nitta et al, 2006), and they have also been reported as induced in corals after treatment with the bacterial immune elicitor MDP (Weiss et al, 2013). In Arabidopsis, IAN/GIMAP proteins are defined by the presence of an avrRpt2-induced gene 1 (AIG1) domain, and contain conserved GTP-binding domains, including a P-loop motif known to bind GTP/GDP in Ras GTPases (Bourne et al, 1991), and coiled-coil motifs (Liu et al, 2008). Originally, *AtAIG1* (also known as *IAN8*) was defined as a gene overexpressed in response to the avirulent bacterial strain *Pseudomonas syringae* pv. *maculicola* (*Pma*) expressing the effector AvrRpt2 (Reuber and Ausubel, 1996). Additionally, computational analysis of transcriptomic data has revealed that the transcription of other *IAN* family members responds to different biotic stimuli: nematode infection induces the expression of *IAN3* and *IAN11*, while the transcription of *IAN11*, *IAN12* and *IAN13* is reduced by infection with *Myzus persicae* (Liu et al, 2008).

Despite the accumulating evidences that associate *IAN* genes with immunity in plants, no characterization of their function in this process has been carried out to date. Here, we analyzed the expression patterns of *IAN* genes and found that the expression of *IAN9* is repressed upon pathogen infection or treatment with immune elicitors. Further characterization indicated that *IAN9* encodes a plasma membrane-localized protein and that it genetically behaves as a negative regulator of immunity. *In vivo* immunoprecipitation of IAN9-GFP followed by mass spectrometry analysis revealed that IAN9 associates with a C3HC4-type RING finger domain-containing protein that we named IAP1, for IAN9-associated protein 1. Interestingly, our results show that IAP1, like IAN9, negatively regulates immunity, raising the idea that these two proteins may work together in the control of immune responses.

Materials and Methods

Plant materials and growth conditions

Arabidopsis seeds were sterilized with bleach solution (20% bleach and 0.1% Triton X-100) for 2-3 minutes, then washed with sterile water 4-5 times and sown on solid ½ MS medium (2.21 g Murashige & Skoog Basal Medium with Vitamins, 15 g Sucrose, 7 g Agar. 1 L). After stratification at 4°C for 3 days, the plates were transferred to a growth chamber (22°C, 16 h light/8 h dark) for germination and growth. For experiments involving mature Arabidopsis plants, sterile seeds were firstly stratified at 4°C for 3 days, then transferred to soil. Plants for bacterial infection assays were cultivated in a short day chamber (22°C, 8 h light/16 h dark photoperiod, 65% humidity). Plants for *Agrobacterium* transformation were grown in a long day growth room (22°C, 16 h light/8 h dark photoperiod).

Bacterial infections

Pseudomonas syringae pv tomato DC3000 (*Pst* DC3000) and DC3000 (AvrRpt2) were streaked on selective ½ salt LB plates (10 g Tryptone, 5 g Yeast Extract, 5 g NaCl, 15 g Agar per 1 L) and cultivated at 22°C for 2 days. For *Pst* DC3000, bacteria were collected from the plates into sterile water, the OD was adjusted to a value of 0.1 ($5x10^7$ cfu/ml) or 0.2 (10^8 cfu/ml), and silwet-L77 was added to a final concentration of 0.03% before performing spray inoculation onto 3-4 week-old soil-grown Arabidopsis under short day conditions. The plants were then covered with cling wrap for 3 hours. The whole plants were harvested in 1.5 ml microcentrifuge tubes and weighed. For *Pst* DC3000 (AvrRpt2), the OD was adjusted to 0.1 ($5x10^7$ cfu/ml) or 0.001 (10^5 cfu/ml). The bacterial suspension was pressure-infiltrated into 5-6 week-old short day-grown Arabidopsis leaves with a needleless syringe (3 leaves per plant), and leaf discs were collected into 1.5 ml tubes using a leaf punch at 3 days post-inoculation. In both cases, plant tissues were ground and homogenized in sterile water before plating serial dilutions on selective ½ salt LB agar plates. The plates were placed at 28°C for 1.5 days and the bacterial growth was calculated as colony-forming units.

Treatments with immune elicitors

Sterile seeds were sown on ½ solid MS medium to germinate and grown for 3-4 days in long day conditions. Seedlings were then transferred into ½ liquid MS medium in 12-well culture plates (Thermo Fisher Scientific, Waltham, MA, US), and grown for another 6-7 days. Every well contained 3 seedlings, and every experiment included 3

independent samples from 3 independent wells. The flg22 peptide or salicylic acid were added into the liquid medium to a final concentration of 100 nM and 0.5 mM, respectively. All the plates were incubated on a shaker for 5-10 minutes following addition of the elicitor. Samples were harvested into 1.5 ml tubes at different time points after treatment, as indicated in the figures.

Root growth assay

Sterile seeds were sown on ½ solid MS medium and stratified at 4°C for 3 days. Then the plates were placed into a growth chamber for 1 day. The germinated seedlings were transferred to the new ½ solid MS medium (square plates). Square plates were placed vertically into a growth chamber and root length was measured 5 days later.

RNA isolation, RT-PCR, and RT-qPCR

For RNA extraction, plant tissues were collected in 1.5 ml microfuge tubes with one metal bead and the tubes were immediately placed into liquid nitrogen. Samples were ground thoroughly with a TissueLyser (QIAGEN, Duesseldorf, Nordrhein-Westfalen, Germany) for 1 minute, and placed back in liquid nitrogen. Total RNA was extracted with the E.Z.N.A. Plant RNA kit (Omega Bio-Tek, Norcross, GA, US) with in-column DNA digestion and an additional sample treatment with DNAase (Omega Bio-Tek, Norcross, GA, US). First-strand cDNA was synthesized using the iScript cDNA synthesis kit (Bio-Rad, Hercules, CA, US) with a volume of 20 µl. For RT-PCR, the PCR reaction was performed in 50 µl using the Q5 Hot Start High-Fidelity DNA polymerase (New England Biolabs, Ipswich, MA, US) with 35 or 38 cycles. For quantitative RT-PCR (RT-qPCR) , PCR reactions were performed in 20 µl using the iTaq Universal SYBR Green Supermix kit (Bio-Rad, Hercules, CA, US) in the StepOnePlus Real-Time PCR System (Applied Biosystems, Foster City, CA, US). Data were analyzed with Excel and GraphPad Prism 6.

Confocal microscopy imaging

Cotyledons from 3-4 day-old long day-grown Arabidopsis seedlings were imaged using a Confocal Laser Scanning Microscope (CLSW) Platform: Leica TCS SP8 (Leica, Mannheim, Germany). The GFP was excited with an argon laser at 488 nm, and its emission was detected at 500-550 nm. For plasmolysis assays, cotyledons were placed into a 1 M NaCl solution on glass slides, and GFP was observed and recorded after 5-10 minutes. For FM4-64 staining, cotyledons from 4 day-old seedlings were cut and soaked into 5 ng/µl FM4-64 solution as described previously

(Beck et al., 2012) for 5 minutes; samples were then transferred to water on glass slides and covered with coverslips. For dual channel simultaneous observation, the fluorescence signal of FM4-64 was excited with an argon laser at 561 nm and its emission was observed at 580-650 nm; the GFP was excited at 488 nm and observed at 500-550 nm. For co-localization assays, 3 week-old *N. benthamiana* leaves were co-infiltrated with *Agrobacterium* GV3101 carrying plasmids to express *RFP-IAN9* and *GFP-IAP1*. Leaves were co-infiltrated with the GV3101 strain carrying plasmids to express *RFP-IAN9* and *GFP* as control. Three-mm leaf discs were punched from the whole leaf 24 hours post infiltration and transferred to water on glass slides. For dual channel image acquisition, GFP and RFP were excited at 488 nm and 561nm respectively; emission was collected at 500-550 nm for GFP and 580-650nm for RFP.

MAPK activation and western blot assays

For protein extraction, Arabidopsis seedlings or leaf discs from *N. benthamiana* were ground with a Tissue Lyser (QIAGEN, Hilden, Nordrhein-Westfalen, Germany). Samples were then re-suspended in lysis buffer [2x loading buffer: 100 mM Tris-HCl (pH 6.8), 10% Glycerol, 2% SDS, 0.03% bromophenol blue], boiled at 95°C for 10 minutes, and centrifuged at 14,000 g for 5 minutes before loading in SDS-PAGE acrylamide gels. Western blots were performed using anti-GFP (Sigma G6795), anti-Luciferase (Sigma L0159), anti-Mouse IgG-Peroxidase (Sigma A2554), and anti-Rabbit IgG-Peroxidase (Sigma A0545).

MAPK activation assays were performed as previously described (Macho et al, 2012), with minor modifications. Briefly, 7 day-old Arabidopsis seedlings grown on solid ½ MS were transferred to water and then treated with 100 nM flg22 for 10 minutes after vacuuming 5 minutes (15 minutes in total). Anti-pMAPK [Phospho-p44/42 MAPK (Erk1/2) (Thr202/Tyr204) XP Rabbit mAb; Cell Signaling 4370] was dissolved in 3% gelatin (Sigma G7041) and used to hybridize the membranes. All membraneswere stained with Ponceau stain (Sangon Biotech, Shanghai, China) to verify equal loading.

ROS burst

ROS burst assays were conducted as previously described (Sang and Macho, 2017). Briefly, 4 mm leaf discs from 5-6 week-old Arabidopsis plants grown in short day conditions were transferred to 96-well microplates (PerkinElmer, Waltham, MA, US) with 100 µl Mili-Q water per well and incubated overnight. Water was then removed and ROS burst was elicited by adding 100 µl of a solution containing 100 ng flg22,

100 µM luminol, and 20 µg/mL horseradish peroxidase. The luminescence was recorded over 40 minutes using a Thermo Scientific VARIOSKAN FLASH (Thermo Fisher Scientific, Waltham, MA, US).

Co-IP and large-scale IP for LC-MS/MS

Leaves from 3-4 week-old *N. benthamiana* plants were co-infiltrated with *Agrobacterium* GV3101 carrying plasmids to express *GFP-IAP1* and *Cluc-IAN9*; leaves co-infiltrated with GV3101 carrying plasmids to express *GFP-AIP1* and *Cluc* or *GFP* and *Cluc* were used as controls. Total proteins were extracted 24 hours later, and immunoprecipitation was performed with GFP-trap beads (Chromotek, Am Klopferspitz, Planegg-Martinsried, Germany) as described previously (Sang et al, 2016). Proteins were stripped from the beads by boiling in 50 µl SDS loading buffer for 10 mins. Immunoprecipitated proteins were separated on SDS-PAGE acrylamide gels and western blots were performed as described above. Large-scale immunoprecipitation assays for LC-MS/MS were performed as described before (Kadota et al. 2016; Sang et al. 2016), using 5 g of 10 day-old Arabidopsis seedlings before or after treatment with 100 nM flg22 or 0.5 mM SA.

Results

Expression analysis of the *IAN* gene family upon bacterial infection reveals differential expression patterns for *IAN7*, *IAN8,* and *IAN9*

The IAN protein family in Arabidopsis is composed of 13 members (Liu et al, 2008; Figure 1A). Phylogenetic analysis of IAN amino acid sequences shows a clear separation in different subgroups (Figure 1A, Figure S1). Previous reports have described changes in expression of *IAN* gene family members upon different biotic stimuli (Reuber and Ausubel, 1996; Liu et al, 2008). In order to characterize the transcriptional response of *IAN* genes to bacterial infection, we inoculated Arabidopsis seedlings with the virulent pathogen *Pseudomonas syringae* pv. *tomato* (*Pst*) DC3000. Three *IAN* genes showed differential expression patterns upon bacterial infection: *IAN7* and *IAN8* showed a significant up-regulation, while *IAN9* showed a significant down-regulation (Figure 1B). Regarding other *IAN* members, we did not detect mRNA for *IAN1/2/4/6/10/11/12/13,* suggesting that these genes are not expressed in 10 day-old Arabidopsis seedlings in our experimental conditions, while transcript abundance for *IAN3/5* was not influenced by pathogen infection (data not shown). The pathogen-induced up-regulation of *IAN8* is reminiscent of the originally reported up-regulation of this gene by bacteria expressing the effector AvrRpt2, which induces activation of the plant NLR RPS2 (Reuber and Ausubel, 1996). Accordingly, we found that the differential expression of *IAN7/8* and *IAN9* also takes place upon infection of Arabidopsis rosette leaves with *Pst* expressing *AvrRpt2* (Figure 1C). The particular expression pattern of *IAN9* among the *IAN* gene family suggests an exclusive function for IAN9 rather than functional redundancy with other IAN family members. This idea is supported by the fact that *IAN9* constitutes a specific phylogenetic group within the *IAN* gene family (Figure 1A). For these reasons, we decided to focus our attention on IAN9.

IAN9 expression is reduced upon chemical activation of plant immunity

IAN9 is broadly expressed in cotyledons, hypocotyls, and roots of Arabidopsis seedlings (Figure S2). To dissect the bacteria-induced repression of *IAN9* transcription, we sought to determine whether perception of purified immune elicitors affects *IAN9* expression. For this purpose, we first treated Arabidopsis seedlings with the flagellin-derived peptide flg22, which is widely used as an elicitor of immune responses. Our results show that *IAN9* expression is significantly reduced one hour after flg22 treatment (Figure 2A). The perception of different invasion patterns, including flg22, leads to the production of the phytohormone salicylic acid (SA),

which is a key player in the activation of plant immunity against biotrophic pathogens (Vlot et al., 2009). Treatment with SA for three hours led to a reduction of *IAN9* expression, although the abundance of *IAN9* transcripts returned to basal levels after a 6-hour SA treatment (Figure 2B), revealing a transient down-regulation of *IAN9* transcript abundance upon SA treatment. Finally, to determine whether the reduction on *IAN9* transcription upon flg22 treatment depends on the downstream SA accumulation (Tsuda et al., 2008), we performed flg22 treatment in the SA-depleted *sid2/NahG* plants, deficient in pathogen-induced SA biosynthesis (Wildermuth et al. 2001) and constitutively expressing the bacterial salicylate hydroxylase NahG, which degrades SA (Delaney et al., 1994). Interestingly, the flg22-triggered down-regulation of *IAN9* transcript abundance was also observed in *sid2/NahG* plants, suggesting that SA is not required for the flg22-induced transcriptional repression of *IAN9*.

IAN9 localizes to the plasma membrane through its C-terminal part

In order to investigate the subcellular localization of IAN9, we generated stable transgenic Arabidopsis lines expressing an N-terminal GFP-tagged IAN9 protein (see below for a detailed characterization of these lines), and used confocal microscopy to determine the localization of GFP-IAN9. Contrary to free GFP, which shows a nuclear/cytoplasmic localization, GFP-IAN9 specifically localized at the cell periphery (Figure 3A). This localization was similar to that observed for well-characterized plasma membrane (PM)-localized proteins, such as the brassinosteroid (BR) receptor BRI1 (Wang et al., 2001; Figure 3A). To determine whether GFP-IAN9 is associated to membranes, we used the lipophilic fluorescent dye FM4-64, which is rapidly incorporated into membranes upon contact with plant cells (Fischer-Parton et al., 2000; Bolte et al., 2004). Our results show that GFP-IAN9 fluorescence co-localizes with FM4-64-labeled compartments (Figure 3B and 3C), similar to BRI1-GFP fluorescence, and different from free GFP (Figure 3B and 3C). To further confirm that IAN9 localizes at the PM, we performed plasmolysis assays by treating plant tissues with 1 M NaCl. Upon plasmolysis, both GFP-IAN9 and BRI1-GFP were detected in Hechtian strands, which are associated to PM retractions from the cell wall (Figure 3D). Altogether, our microscopy analysis indicates that IAN9 localizes at the PM in plant cells.

The C-terminal domain is not conserved among IAN proteins (Figure S1). Interestingly, the C-terminal sequence of IAN9 shows an over-representation of positively charged amino acids (KKLRENLERAEKETKELQKKLGKCINL; 33.3% of R/K), not present in other IAN proteins (Figure S1 and S3A), which could mediate an interaction with the negatively charged phospholipids of the PM. To test this

hypothesis, we generated Arabidopsis stable transgenic lines expressing a truncated GFP-IAN9 version lacking the 27 C-terminal amino acids (IAN9ΔC-27). The IAN9ΔC-27 version lost the specific PM localization seen for wild type GFP-IAN9, and was mostly detected in the cytoplasm (Figure S3B). Additionally, we found that, when GFP is fused to the C-terminal end of IAN9 (IAN9-GFP), this protein loses its specific PM localization, and is mostly found in the cytoplasm (Figure S3B). Compared to IAN9, the IAN8 C-terminal part has a lower representation of positively charged aminoacids (18.5%; Figure S3A), and we found that a N-terminal GFP-tagged IAN8 (GFP-IAN8) localizes to the cytoplasm. Altogether, these results suggest that the exclusive C-terminal domain of IAN9 is required for its localization at the PM.

Generation of *IAN9* knock-out and overexpression lines

Public repositories for Arabidopsis T-DNA insertion lines contain four independent lines with T-DNA insertions in the *IAN9* genomic locus: *SAIL_167_B02*, *SALK_534_B01*, *SALK_144369,* and *GK-146B08*. For all these lines, the insertion site is located in the predicted promoter region of *IAN9*. Among them, *GK-146B08* is the line harboring the nearest T-DNA insertion to the *IAN9* start codon (Figure S4A), and therefore we chose this line for further analyses. Sequencing analysis results showed that the insertion site is located 76 bp upstream of the 5'-UTR of the *IAN9* gene, and 319 bp upstream of the *IAN9* start codon (Figure S4A and S4B). RT-PCR and RT-qPCR analyses showed that this mutant has approximately a 3-fold reduction in the amount of *IAN9* transcripts (Figure S4C and S4D), indicating that this line is a knockdown *ian9* mutant. To further characterize this line, we determined the *IAN9* transcript levels upon bacterial inoculation. Surprisingly, we found that *IAN9* transcript levels increased significantly upon inoculation with *Pst* or *Pst* (AvrRpt2), reaching higher levels than those observed in wild type plants (Figure S4E) and an opposite regulation (Figure 1). These findings indicate that the T-DNA insertion in the *IAN9* promoter generates an aberrant expression pattern of *IAN9* in this line, rendering it unusable for the functional characterization of this gene.

In order to perform genetic analysis of the contribution of IAN9 to plant immunity, we generated *ian9* mutant lines using CRISPR/Cas9-assisted genome editing (Feng et al, 2013; Mao et al, 2013). We selected the best predicted target site in the *IAN9* gene sequence for recognition by the Cas9/sgRNA complex (Figure S5), and performed the targeted mutagenesis as explained in the methods section. Sequencing of the resulting line showed an addition of 1 base pair in the second exon of *IAN9*, creating a premature stop codon 366 base pairs downstream of the start codon (Figure S6A), which generates a truncated protein with a disrupted GTP-

binding domain. Upon selection of seedlings containing the *ian9* mutation in homozygosis, we selected a line for which where the Cas9 gene was segregated out (Figure S6B); this Cas9-free *ian9* line was used for further experiments. Additionally, as mentioned before, we generated Arabidopsis transgenic lines overexpressing *IAN9* in a Col-0 wild type background, using a 35S promoter to express a *GFP-IAN9* fusion. We selected two independent homozygous lines that accumulated detectable amounts of GFP-IAN9 fusion protein (Figure S6C), and higher transcript levels of *IAN9* compared to those in Col-0 wild type (OE-*GFP-IAN9#3-10* and OE-*GFP-IAN9#7-1*) (Figure S6D). As controls, we selected two independent homozygous lines expressing free GFP, which did not show changes in *IAN9* transcription and accumulated detectable levels of free GFP (Figure S6C and S6D). Interestingly, although the 35S promoter led to high *IAN9* expression compared to Col-0 wild type, bacterial infection still caused a reduction in *IAN9* transcript levels (Figure S7), suggesting a post-transcriptional regulation of the abundance of *IAN9* transcripts. Overexpression of *IAN9* did not affect *IAN8* expression in basal conditions or upon bacterial infection (Figure S7).

Plant growth and early immune responses are not affected by altered expression of *IAN9*

Both *IAN9* overexpressing or *ian9* knockout seedlings and adult plants were visually indistinguishable from the wild type (Figure S8 and S9). Given the predicted association of the IAN family to immune responses and the alteration in *IAN9* expression upon elicitation with flg22, we sought to determine whether IAN9 is involved in early PTI responses, namely the flg22-triggered burst of reactive oxygen species (ROS), and the activation of a cascade of mitogen-activated protein kinases (MAPKs) (Boller & Felix, 2009, Macho & Zipfel, 2014). Our results show that mutation or overexpression of *IAN9* did not have a detectable impact in the dynamics or total accumulation of ROS upon flg22 treatment (Figure S8B, S8C and Figure S10). Similarly, neither mutant nor overexpression (OE) lines showed differences in flg22-triggered MAPK activation compared to wild type plants or free GFP-expressing controls (Figure S8D and S8E). Taken together, these results suggest that alterations of *IAN9* expression do not affect early PTI responses.

IAN9 negatively regulates plant immunity against *Pst* DC3000

To test whether IAN9 contributes to plant immunity against bacterial pathogens, we performed surface inoculation of the *ian9* mutant line with *Pst* DC3000 and determined bacterial replication in plant tissues. Our results show that knockout

mutation of *IAN9* increased plant resistance against *Pst* DC3000, causing a 13-fold reduction on bacterial titers (Figure 4A). In order to test whether the increase in resistance also occurs in a context of ETI, we syringe-infiltrated Arabidopsis rosette leaves with *Pst* (AvrRpt2). However, no differences were detected in terms of replication of this strain (Figure 4B). To confirm that the observed increased resistance to *Pst* DC3000 is really due to the absence of *ian9*, we generated complementation lines expressing *GFP-IAN9*, driven by a *35S* promoter, in the *ian9* knockout mutant background, where the GFP-IAN9 protein accumulated and localized to the PM (Figure S11A and S11B). Expression of GFP-IAN9 in the *ian9* background was able to rescue the level of growth of *Pst* DC3000 to that observed in wild type plants (Figure S11C), confirming the association of IAN9 with the observed increased resistance. Interestingly, transgenic lines overexpressing GFP-IAN9 in a wild type background showed a tendency to support higher bacterial loads compared to wild type or GFP-expressing lines, suggesting that IAN9 overexpression suppresses plant immunity against *Pst* DC3000, although such tendency was not always reproducible or statistically significant across eight independent biological repeats (Figure S12).

Identification of IAN9-interacting proteins

To characterize further the mode of action of IAN9, we searched for proteins physically associated with IAN9 in plant cells using Arabidopsis seedlings expressing *GFP-IAN9* (line OE-*GFP-IAN9#3-10*) and seedlings expressing free GFP as control. Upon GFP immunoprecipitation (IP) using agarose beads coupled to an anti-GFP nanobody (GFP-Trap beads), we detected associated proteins using liquid chromatography coupled to tandem mass-spectrometry (LC-MS/MS). In order to detect potential dynamic interactions, we additionally treated seedlings for one hour with flg22 or SA before immunoprecipitation. Two independent biological replicates showed a large number of proteins physically associated with IAN9, which we filtered using the following criteria: 1. Presence in both biological replicates; 2. Detection of two or more exclusive unique peptides; 3. Absence in the GFP control. After applying these filters, a total of 14 proteins were identified as IAN9 candidate interactors (Table S1).

Among these candidate interactors, we drew our attention to an uncharacterized protein encoded by the AT1G18660 gene (Table S1), which we named IAP1 for IAN9-ASSOCIATED PROTEIN1. Interestingly, IAP1 associated with IAN9 in both replicates of IP + LC-MS/MS, but the number of detected IAP1 peptides decreased in

456 samples treated with SA, while it did not change significantly in samples treated with
457 flg22 (Table S1). Domain analysis predicts the presence of three tetratricopeptide-
458 like helical (TPR) domains, a C3HC4-type RING finger domain, and an ATP-
459 dependent protease La (LON) domain in this protein (Figure S13A). Upon
460 Agrobacterium-mediated transient expression in *Nicotiana benthamiana*, a GFP-IAP1
461 fusion protein localized at the cell periphery, nucleus (weakly), and around the
462 nucleus; the latter most likely corresponds to the usual endoplasmic reticulum
463 localization of PM-localized proteins overexpressed in this system (Figure S13B and
464 S13C). Co-expression with RFP-IAN9 showed that both proteins co-localize upon
465 transient expression (Figure 5A). To confirm the interaction between IAN9 and IAP1,
466 we performed a targeted co-IP using GFP-IAP1 and a N-terminal fusion of IAN9 to
467 the C-terminal domain of luciferase (Cluc-IAN9). Co-IP assays show that GFP-IAP1
468 interacts with Cluc-IAN9, but not with Cluc alone (Figure 5B); Cluc-IAN9 does not
469 interact with free GFP (Figure S14). To determine whether the IAN9-IAP1 interaction
470 is direct, we performed a luciferase complementation assay, transiently co-
471 expressing Cluc-IAN9 and IAP1 fused to the N-terminal domain of luciferase (IAP1-
472 Nluc). A positive control co-expressing AtSGT1b-Nluc and Cluc-AtRAR1 showed a
473 strong luciferase signal (Figure S15A), as described before (Chen et al., 2008). On
474 the contrary, tissues co-expressing Cluc-IAN9 and Nluc-IAP1 did not show any
475 detectable luciferase signal (Figure S15A), although both proteins accumulated
476 (Figure S15B). As an alternative technique to detect direct interactions, we employed
477 FRET-FLIM by co-expressing GFP-IAP1 and RFP-IAN9. However, no difference in
478 GFP fluorescence lifetime was detected when compared to control samples (Figure
479 S15C). Although an influence of the tags cannot be ruled out, these results suggest
480 that the interaction observed for IAP1 and IAN9 is most likely indirect.
481
482 **IAP1 negatively regulates plant immunity against *Pst* DC3000**
483 Public repositories for Arabidopsis T-DNA insertion lines contain two independent
484 lines with T-DNA insertions in the *IAP1* genomic locus: *SALK_119114* and
485 *SALK_093498* (Figure S16A). We isolated homozygous lines containing these
486 insertions (Figure S16B) and confirmed the absence of *IAP1* transcripts (Figure
487 S16C), naming these lines *iap1-1* and *iap1-2*, respectively (Figure S16A). Both lines
488 displayed wild-type-like growth and development when grown on soil under short-day
489 conditions (Figure 6A), although mutant seedlings showed a slightly reduced root
490 length compared to Col-0 wild type when grown in vertical MS plates (Figure S17).
491 To determine whether mutations in *IAP1* have an impact on plant resistance against
492 bacterial pathogens, we performed surface inoculation of the *iap1* mutant lines with

493 *Pst* DC3000. Our results show that both *iap1-1* and *iap1-2* mutant lines are more
494 resistant than Col-0 wild type against *Pst* DC3000, showing a 19-fold reduction on
495 bacterial loads (Figure 6B). However, none of these lines showed differences after
496 inoculation with *Pst* expressing AvrRpt2 (Figure 6C). Interestingly, these results
497 resemble those obtained during the characterization of the *ian9* knockout mutant line
498 (Figure 4), suggesting that both proteins are involved in the negative regulation of
499 basal immunity against bacterial pathogens, and may act in the same pathway
500 through physical association.
501

Discussion

In this work, we characterized the transcription patterns of *IAN* family members in Arabidopsis upon infection with the bacterial pathogen *Pto DC3000*. *IAN7* and *IAN8*, which seem to form a separate phylogenetic subgroup, are up-regulated upon bacterial infection. On the contrary, *IAN9* seems to form a specific subgroup and shows a unique down-regulation upon bacterial infection. Infection with a virulent bacterial pathogen, such as *Pto DC3000*, triggers changes in plant cells caused by bacterial virulence activities (e.g. alteration of plant processes by T3Es) and basal immune responses. Therefore, formally, transcriptional changes upon infection could be associated with bacterial virulence or plant immunity. In this case, the down-regulation of *IAN9* expression upon bacterial infection seems associated with the activation of immunity, since we detected similar expression patterns upon treatment with elicitors of immunity, namely flg22 and SA. Interestingly, we detected a reduction in the amount of *IAN9* transcripts after bacterial infection even in transgenic lines where *IAN9* overexpression is driven by a constitutive *35S* promoter, suggesting a post-transcriptional regulation of *IAN9* transcript abundance. Although the perception of flg22 leads to the production of SA (Tsuda et al., 2008), our data show that the flg22-triggered reduction of *IAN9* transcription takes place in *sid2/NahG* plants, indicating that this transcriptional change is independent of the observed SA-triggered reduction of *IAN9* transcription. SA-deficient mutants are partially affected in flg22-triggered induction of defence-related genes, probably caused by lower levels of the flg22 receptor FLS2 (Yi et al., 2014). Our results indicate that these lower levels of FLS2 in *sid2/NahG* plants are nevertheless sufficient to trigger the *IAN9* transcriptional repression, suggesting that *IAN9* transcription may be highly sensitive to external biotic stimuli.

Besides showing different expression patterns, the subcellular localization of IAN9 (mostly at the PM) is also different from that of IAN8 (mostly in the cytoplasm). This differential localization further suggests distinct functions for these two IAN family members. The C-terminal domain of IAN9, required for PM localization, is not present in other IAN proteins. This could indicate that the IAN9 mechanism for PM attachment is exclusive within the IAN family, although other IAN proteins could localize at the PM through different means.

Mutation of *IAN9* causes increased resistance to *Pto* DC3000, and this phenotype is rescued in complementation lines. It is worth considering the possibility that IAN9 is

guarded by NLRs as it has been shown for some regulators of immunity (Khan et al, 2016), therefore explaining the increased resistance in the *ian9* knockout mutant. However, the absence of developmental phenotypes or constitutive immune responses makes this possibility unlikely. Additionally, overexpression lines show a tendency for increased susceptibility, although this phenotype was not always significant or reproducible. The lack of robustness in this phenotype could suggest that *IAN9* transcript abundance is not rate limiting; however, it could also be due to the potential post-transcriptional regulation of *IAN9* transcript abundance that we have seen in the *IAN9* overexpression lines, which show a reduction in the amount of *IAN9* transcripts after bacterial infection. The transient nature of *IAN9* transcriptional repression upon SA treatment, returning to basal levels after 6 hours, may indicate that the negative regulation exerted by IAN9 could be required to contribute to the repression of immune responses after immunity has been established.

Using IP followed by LC-MS/MS, we found IAP1 as a protein associated with IAN9. IAP1 contains three tetratricopeptide-like helical (TPR) domains, a C3HC4-type RING finger domain, and an ATP-dependent protease La (LON) domain. Upon transient expression, IAP1 co-localizes with IAN9 in *N. benthamiana* cells. Genetic analysis indicates that both IAN9 and IAP1 negatively regulate immunity against *Pto* DC3000. Given their physical association, it is possible that both proteins belong to a protein complex involved in the negative regulation of basal immunity against bacterial pathogens. Although we confirmed the association between IAN9 and IAP1 using targeted IP, we failed to detect a direct physical interaction using luciferase complementation or FRET-FLIM assays. Specific limitations of interaction techniques may be hindering the detection of a direct interaction; however, these data may also indicate that the interaction between IAN9 and IAP1 is indirect, perhaps mediated by other scaffolding components in the same protein complex. The Arabidopsis Interactome Database (http://interactome.dfci.harvard.edu/A_thaliana/index.php) has reported several interactors for IAP1 in Y2H assays (Table S2). Interestingly, several of these interacting proteins are transcription factors, and others have predicted nuclear localization or undergo nucleo-cytoplasmic re-localization associated to their activity (Table S2). Considering that IAP1 interacts with several proteins with nuclear activities, it is tempting to speculate that the IAN9/IAP1 complex could associate with transcriptional regulators in the absence of biotic stress, acting as negative regulators of immune responses, and the complex may dissociate upon pathogen infection to allow for the activation of executor immune responses that restrict pathogen proliferation. This hypothetical model is in agreement with the observation

576 that IAN9 does not seem to regulate early elicitor-induced responses (namely flg22-
577 triggered ROS burst and MAPK activation). Given that *ian9* or *iap1* mutants do not
578 show auto-immunity phenotypes, the final activation of immune responses may
579 require additional activation by other immune regulators, of which the activity could
580 be facilitated by the absence of IAN9 or IAP1.
581
582 Altogether, our results reveal IAN9 and IAP1 as suitable targets for biotechnological
583 approaches to generate crops with increased disease resistance to bacterial
584 pathogens, since both IAN9 and IAP1 have orthologs in agriculturally important crop
585 species (Figure S18 and S19). Current regulations hinder the use of transgenic
586 plants to generate disease-resistant crops. Alternative strategies consider the
587 mutation of negative regulators of immunity, although this often leads to fitness costs
588 or auto-immunity phenotypes, which obstruct their applicability in agriculture.
589 Interestingly, IAN9 and IAP1 behave as negative regulators of basal immunity, since
590 *ian9* and *iap1* knockout plants show increased resistance to bacterial infection, but
591 they do not show obvious differences compared to wild-type plants in terms of size or
592 development. Our *IAN9* mutagenesis approach shows that it is feasible to design
593 CRISPR/Cas9-mediated strategies to obtain stable non-transgenic mutant plants
594 with increased resistance to pathogens and no obvious developmental defects,
595 paving the way to a potential application in breeding for disease resistance.
596

Acknowledgements

We thank members of the Macho and Lozano-Durán laboratories for helpful discussions; Jianming Li, Jian-Min Zhou and Jian-Kang Zhu for sharing biological materials; and Xinyu Jian for technical and administrative assistance during this work. We thank the PSC Cell Biology core facility for assistance with confocal microscopy, and the PSC Proteomics core facility for LC-MS/MS analysis. This work was supported by the Shanghai Center for Plant Stress Biology (Chinese Academy of Sciences). Research in the Macho laboratory is also supported by the National Natural Science Foundation of China (NSFC; grant 31571973) and the Chinese 1000 Talents Program. Research in the Lozano-Durán laboratory is also supported by the National Natural Science Foundation of China (NSFC; grant 31671994) and the 100 Talents Program from the Chinese Academy of Sciences. CCM is sponsored by a CAS-TWAS President's Fellowship for International PhD Students. TR-D is the recipient of a President's International Fellowship Initiative (PIFI) postdoctoral fellowship (No. 2016PB042) from the Chinese Academy of Sciences. The authors have no conflict of interest to declare.

Supplementary data

Figure S1. Alignment of IAN proteins.

Figure S2. Expression of *IAN9* in *Arabidopsis* seedlings.

Figure S3. The C-terminal region of IAN9 is important for its PM localization.

Figure S4. Characterization of the GK-146B08 line with an insertion in the promoter of *IAN9*.

Figure S5. Exact mutation site in the *ian9* mutant generated by CRISPR/Cas9.

Figure S6. Characterization of the *ian9* mutant and *IAN9* over-expression lines.

Figure S7. Transcription of *IAN8* is not affected by over-expression of *IAN9*.

Figure S8. Plant growth and early immune responses are not affected by altered expression of *IAN9*.Figure S9. Seedlings of the *ian9* mutant and *IAN9* over-expression do not show developmental defects.

Figure S10. Flg22-triggered ROS dynamics are not affected by alterations in *IAN9* expression.

Figure S11. Analysis of the *ian9/35S::GFP-IAN9* complementation line.

Figure S12. Transgenic lines overexpressing GFP-IAN9 in a wild type background show a tendency to support higher bacterial loads compared to wild type or GFP-expressing lines.

Figure S13. Characterization of IAP1.

Figure S14. Cluc-IAN9 associates with GFP-IAP1 but not with free GFP in *N. benthamiana* leaves.

Figure S15. IAN9 and IAP1 do not interact directly in *N. benthamiana* leaves.

Figure S16. Characterization of the *iap1* mutant alleles.

Figure S17. Seedlings of the *iap1* mutant lines show slightly reduced root elongation.

Figure S18. *IAN9* orthologs in different plant species.

Figure S19. *IAP1* orthologs in different plant species.

Table S1. Proteins associated to GFP-IAN9 identified after affinity purification followed by LC-MS/MS analysis.

Table S2. IAP1 interactors according to the Arabidopsis Interactome Database.

Table S3. List of primers used in this study

Methods S1

650 **Figure Legends**

651

652 **Figure 1. Transcription patterns of the *IAN* gene family in Arabidopsis.**

653 (A) Phylogenetic tree of IAN proteins. (B and C) Relative expression of *IAN7, IAN8*
654 and *IAN9* in 9-10 days-old Arabidopsis seedlings, 6 hours after inoculation with *Pst*
655 DC3000 (B) or *Pst* DC3000 (AvrRpt2) (C). Real-time quantitative PCR results were
656 normalized with *UBIQUITIN 10* (*UBQ10*, AT4G05320). Values are means ± SEM
657 (n=3). Statistical differences were calculated using one-way ANOVA ($p<0.01$). Each
658 experiment was performed three times with similar results.

659

660 **Figure 2. Treatment with flg22 or salicylic acid causes a reduction on the**
661 **transcription of *IAN9*.**

662 Relative expression of *IAN9* in 9-10 days-old Arabidopsis seedlings. Seedlings in (A)
663 and (C) were treated with 100 nM flg22 for 1 hour. Seedlings in (B) were treated with
664 0.5 mM salicylic acid for 3 or 6 hours. Real-time quantitative PCR results were
665 normalized with *UBIQUITIN 10* (*UBQ10*, AT4G05320). Values are means ± SEM
666 (n=3). Statistical differences were calculated using one-way ANOVA ($p<0.01$). Each
667 experiment were performed three times with similar results.

668

669 **Figure 3. GFP-IAN9 localizes to the plasma membrane in *Arabidopsis***

670 (A) Confocal images of GFP, GFP-IAN9, and BRI1-GFP in *Arabidopsis* cotyledon
671 epidermal cells. Bar=10 μm. (B) Confocal images of GFP, GFP-IAN9, and BRI1-GFP
672 in *Arabidopsis* cotyledon epidermal cells. *Arabidopsis* seedlings were treated FM4-64
673 for 5 minutes before confocal imaging, and the FM4-64 signal is shown in red. Bar=5
674 μm. (C) Fluorescence intensity through the thin lines shown in (B). (D) Confocal
675 images of GFP, GFP-IAN9, and BRI1-GFP in *Arabidopsis* cotyledon epidermal cells
676 after plasmolysis (5-minute treatment with 1M NaCl). Red arrows indicate the
677 presence of Hectian strands. Bar=10 μm.

678

679 **Figure 4. IAN9 negatively regulates plant immunity against *Pst* DC3000.**

680 (A) Growth of surface (spray)-inoculated *Pto* DC3000 (OD_{600}=0.1) in wild-type (WT)
681 Col-0 and *ian9* mutant plants, 3 days post-inoculation (dpi). Experiments repeated
682 more than three times with similar results. (B) Growth of *Pto* DC3000 (AvrRpt2)
683 (OD_{600}=0.001) infiltrated with a needleless syringe into wild-type (WT) Col-0 and *ian9*
684 mutant plants, 3 days post-inoculation (dpi). Experiments performed twice with
685 similar results. (A and B) Data were represented as means ± SE (n=8). Statistical

differences were calculated using a Student's t-test. "ns" indicates no significant difference, and asterisk indicated significant difference ($p<0.05$).

Figure 5. IAP1 interacts with IAN9 in *N. benthamiana* leaves.

(A) Confocal microscopy images showing the co-localization of GFP-IAP1 and RFP-IAN9 in *N. benthamiana* leaves. Bar=10 μm. (B) Cluc or Cluc-IAN9 was co-expressed with GFP-IAP1 in *N. benthamiana* before immunoprecipitation using GFP-trap beads. Immunoblots were analysed using anti-luc or anti-GFP antibody. Molecular weight (kDa) marker bands are indicated for reference. The experiments were repeated three with similar results.

Figure 6. IAP1 negatively regulates plant immunity against *Pst* DC3000.

(A) Photography of four week-old Col-0 wild type (WT), *iap1-1*, and *iap1-2* plants, grown at a 8 h light/16 h dark photoperiod. Scare bar is 0.5 cm. (B) Growth of surface (spray)-inoculated *Pto* DC3000 (OD_{600}=0.1) in wild-type (WT) Col-0, *iap1-1,* and *iap1-2* mutant plants, 3 days post-inoculation (dpi). Experiments repeated more than three times with similar results. (C) Growth of *Pto* DC3000 (AvrRpt2) (OD_{600}=0.001) infiltrated with a needleless syringe into wild-type (WT) Col-0, *iap1-1,* and *iap1-2* mutant plants, 3 days post-inoculation (dpi). Experiments performed twice with similar results. (B and C) Data were represented as means ± SE (n=8). Statistical differences were calculated using a Student's t-test. "ns" indicates no significant difference, and asterisk indicated significant difference ($p<0.05$).

Bibliography

Beck M, Zhou J, Faulkner C, MacLean D, Robatzek S. 2012. Spatio-temporal cellular dynamics of the Arabidopsis flagellin receptor reveal activation status-dependent endosomal sorting. *Plant Cell* 24: 4205-4219.

Bigeard J, Colcombet J, Hirt H. 2015. Signaling mechanisms in pattern-triggered immunity (PTI). *Mol Plant* 8: 521-539.

Boller T, Felix G. 2009. A Renaissance of Elicitors: Perception of Microbe-Associated Molecular Patterns and Danger Signals by Pattern-Recognition Receptors. Annu Rev *Plant Biol* 60: 379-406.

Bolte S, Talbot C, Boutte Y, Catrice O, Read ND, Satiat-Jeunemaitre B. 2004. FM-dyes as experimental probes for dissecting vesicle trafficking in living plant cells. *J Microsc* 214: 159-173.

Bourne HR, Sanders DA, McCormick F. 1991. The GTPase superfamily: conserved structure and molecular mechanism. *Nature* 349: 117-127.

Campos ML, Yoshida Y, Major IT, de Oliveira Ferreira D, Weraduwage SM, Froehlich JE, Johnson BF, Kramer DM, Jander G, Sharkey TD and Howe GA. (2016). Rewiring of jasmonate and phytochrome B signalling uncouples plant growth-defense tradeoffs. *Nature Comms*, 7, 12570.

Chen H, Zou Y, Shang Y, Lin H, Wang Y, Cai R, Tang X, Zhou JM. 2008. Firefly luciferase complementation imaging assay for protein-protein interactions in plants. *Plant Physiol* 146: 368-376.

Chiang YH, Coaker G. 2015.Effector Triggered Immunity: NLR Immune Perception and Downstream Defense Responses. *The Arabidopsis Book*. American Society of Plant Biologists, 13: e0183.

Clough SJ, Bent AF. 1998. Floral dip: a simplified method for Agrobacterium-mediated transformation of Arabidopsis thaliana. *Plant J* 16: 735-743.

751 Cook DE, Mesarich CH, Thomma BPHJ. 2015. Understanding Plant Immunity as a
752 Surveillance System to Detect Invasion. *Annual Review of Phytopathology*, Vol 53:
753 541-563.
754
755 Couto D, Zipfel C. 2016. Regulation of pattern recognition receptor signalling in
756 plants. *Nat Rev Immunol* 16: 537-552.
757
758 de Wit M, Spoel SH, Sanchez-Perez GF, Gommers CMM, Pieterse CMJ, Voesenek
759 LACJ, Pierik R. 2013. Perception of low red:far-red ratio compromises both salicylic
760 acid- and jasmonic acid-dependent pathogen defences in Arabidopsis. *Plant J* 75:
761 90-103.
762
763 Delaney TP, Uknes S, Vernooij B, Friedrich L, Weymann K, Negrotto D, Gaffney T,
764 Gut-Rella M, Kessmann H, Ward E, et al. 1994. A central role of salicylic Acid in
765 plant disease resistance. *Science* 266: 1247-1250.
766
767 Feng Z, Zhang B, Ding W, Liu X, Yang DL, Wei P, Cao F, Zhu S, Zhang F, Mao Y, et
768 al. 2013. Efficient genome editing in plants using a CRISPR/Cas system. *Cell Res*
769 23: 1229-1232.
770
771 Fischer-Parton S, Parton RM, Hickey PC, Dijksterhuis J, Atkinson HA, Read ND.
772 2000. Confocal microscopy of FM4-64 as a tool for analysing endocytosis and
773 vesicle trafficking in living fungal hyphae. *J Microsc* 198: 246-259.
774
775 Huot B, Yao J, Montgomery BL, He SY. 2014. Growth-defense tradeoffs in plants: a
776 balancing act to optimize fitness. *Mol Plant* 7: 1267-1287.
777
778 Kadota Y, Macho AP, Zipfel C. 2016. Immunoprecipitation of Plasma Membrane
779 Receptor-Like Kinases for Identification of Phosphorylation Sites and Associated
780 Proteins. *Methods Mol Biol* 1363: 133-144.
781
782 Khan M, Subramaniam R, Desveaux D. 2016. Of guards, decoys, baits and traps:
783 pathogen perception in plants by type III effector sensors. *Curr Opin Microbiol* 29: 49-
784 55.
785

786 Liu C, Wang T, Zhang W, Li X. 2008. Computational identification and analysis of
787 immune-associated nucleotide gene family in Arabidopsis thaliana. *J Plant Physiol*
788 165: 777-787.
789
790 Macho AP. 2016. Subversion of plant cellular functions by bacterial type-III effectors:
791 beyond suppression of immunity. *New Phytol* 210: 51-57.
792
793 Macho AP, Boutrot F, Rathjen JP, Zipfel C. 2012. Aspartate oxidase plays an
794 important role in Arabidopsis stomatal immunity. *Plant Physiol* 159: 1845-1856.
795
796 Macho AP, Zipfel C. 2014. Plant PRRs and the activation of innate immune signaling.
797 *Mol Cell* 54: 263-272.
798
799 Macho AP, Zipfel C. 2015. Targeting of plant pattern recognition receptor-triggered
800 immunity by bacterial type-III secretion system effectors. *Curr Opin Microbiol* 23: 14-
801 22.
802
803 Mao Y, Zhang H, Xu N, Zhang B, Gou F, Zhu JK. 2013. Application of the CRISPR-
804 Cas system for efficient genome engineering in plants. *Mol Plant* 6: 2008-2011.
805
806 Nakagawa T, Kurose T, Hino T, Tanaka K, Kawamukai M, Niwa Y, Toyooka K,
807 Matsuoka K, Jinbo T, Kimura T. 2007. Development of series of gateway binary
808 vectors, pGWBs, for realizing efficient construction of fusion genes for plant
809 transformation. *J Biosci Bioeng* 104: 34-41.
810
811 Nitta T, Nasreen M, Seike T, Goji A, Ohigashi I, Miyazaki T, Ohta T, Kanno M,
812 Takahama Y. 2006. IAN family critically regulates survival and development of T
813 lymphocytes. *PLoS Biol* 4: e103.
814
815 Nitta T, Takahama Y. 2007. The lymphocyte guard-IANs: regulation of lymphocyte
816 survival by IAN/GIMAP family proteins. *Trends Immunol* 28: 58-65.
817
818 Reuber TL, Ausubel FM. 1996. Isolation of Arabidopsis genes that differentiate
819 between resistance responses mediated by the RPS2 and RPM1 disease resistance
820 genes. *Plant Cell* 8: 241-249.
821

822 Sang Y, Macho AP. 2017. Analysis of PAMP-Triggered ROS Burst in Plant Immunity.
823 *Methods Mol Biol* 1578: 143-153.
824
825 Sang Y, Wang Y, Ni H, Cazale AC, She YM, Peeters N, Macho AP. 2016. The
826 Ralstonia solanacearum type III effector RipAY targets plant redox regulators to
827 suppress immune responses. *Mol Plant Pathol*.
828
829 Scheres B, van der Putten WH. 2017. The plant perceptron connects environment to
830 development. *Nature* 543: 337-345.
831
832 Stael S, Kmiecik P, Willems P, Van Der Kelen K, Coll NS, Teige M, Van Breusegem
833 F. 2015. Plant innate immunity--sunny side up? *Trends Plant Sci* 20: 3-11.
834
835 Takai Y, Sasaki T, Matozaki T. 2001. Small GTP-binding proteins. *Physiol Rev* 81:
836 153-208.
837
838 Tsuda K, Glazebrook J, Katagiri F. 2008. The interplay between MAMP and SA
839 signaling. *Plant Signal Behav* 3: 359-361.
840
841 Vernoud V, Horton AC, Yang Z, Nielsen E. 2003. Analysis of the small GTPase gene
842 superfamily of Arabidopsis. *Plant Physiol* 131: 1191-1208.
843
844 Vlot AC, Dempsey DA, Klessig DF. 2009. Salicylic Acid, a multifaceted hormone to
845 combat disease. *Annu Rev Phytopathol* 47: 177-206.
846
847 Wang ZY, Seto H, Fujioka S, Yoshida S, Chory J. 2001. BRI1 is a critical component
848 of a plasma-membrane receptor for plant steroids. *Nature* 410: 380-383.
849
850 Weiss Y, Foret S, Hayward DC, Ainsworth T, King R, Ball EE, Miller DJ. 2013. The
851 acute transcriptional response of the coral Acropora millepora to immune challenge:
852 expression of GiMAP/IAN genes links the innate immune responses of corals with
853 those of mammals and plants. *BMC Genomics* 14: 400.
854
855 Wildermuth MC, Dewdney J, Wu G, Ausubel FM. 2001. Isochorismate synthase is
856 required to synthesize salicylic acid for plant defence. *Nature* 414: 562-565.
857

Win J, Chaparro-Garcia A, Belhaj K, Saunders DG, Yoshida K, Dong S, Schornack S, Zipfel C, Robatzek S, Hogenhout SA, et al. 2012. Effector biology of plant-associated organisms: concepts and perspectives. *Cold Spring Harb Symp Quant Biol* 77: 235-247.

Yi SY, Shirasu K, Moon JS, Lee SG, Kwon SY. 2014. The activated SA and JA signaling pathways have an influence on flg22-triggered oxidative burst and callose deposition. *PLoS One* 9: e88951.

Zipfel C. 2014. Plant pattern-recognition receptors. *Trends Immunol* 35: 345-351.

Figure 1

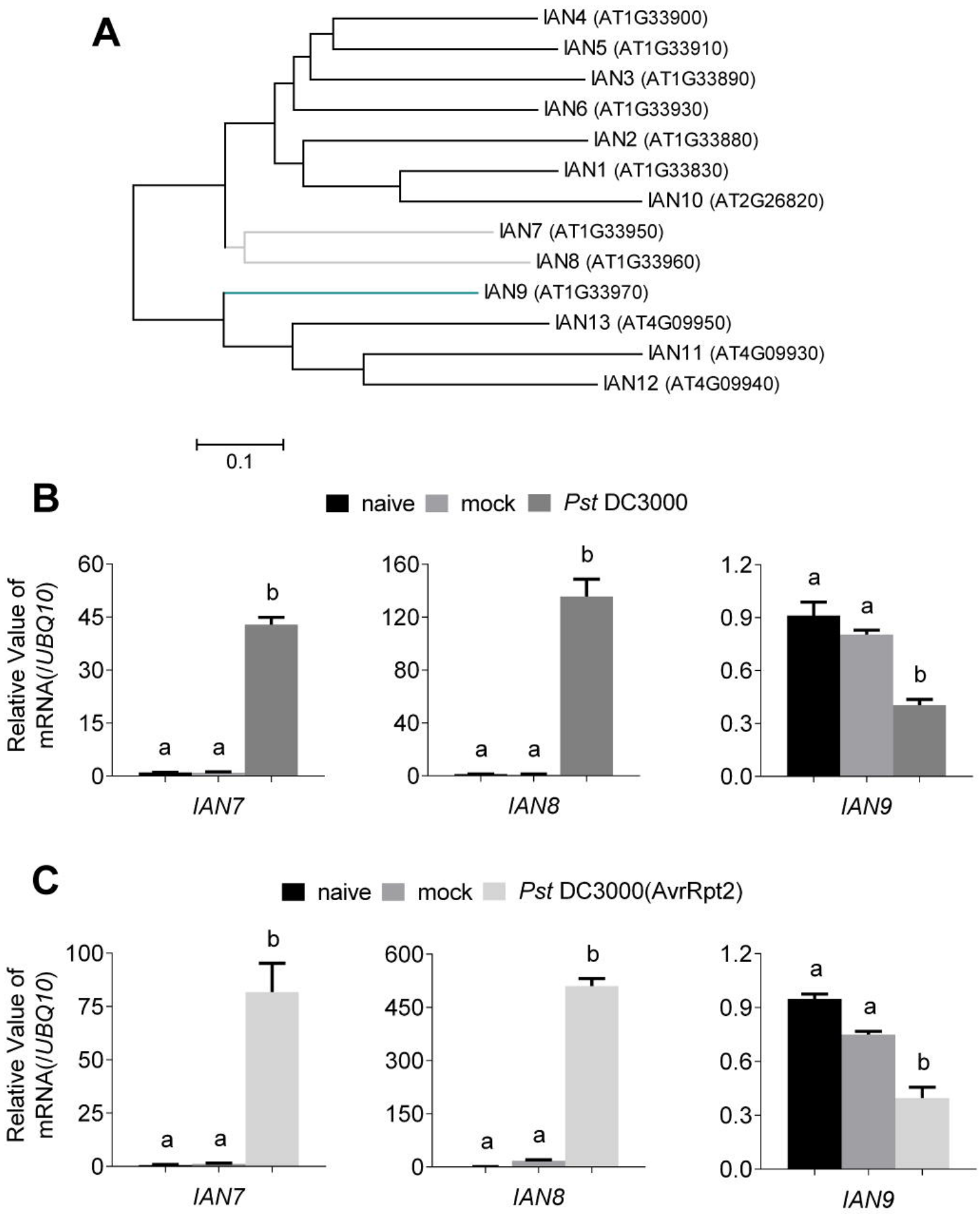
A
IAN4 (AT1G33900)
IAN5 (AT1G33910)
IAN3 (AT1G33890)
IAN6 (AT1G33930)
IAN2 (AT1G33880)
IAN1 (AT1G33830)
IAN10 (AT2G26820)
IAN7 (AT1G33950)
IAN8 (AT1G33960)
IAN9 (AT1G33970)
IAN13 (AT4G09950)
IAN11 (AT4G09930)
IAN12 (AT4G09940)
0.1
B
naive
mock
Pst DC3000
Relative Value of mRNA(IUBQ10)
IAN7
IAN8
IAN9
C
naive
mock
Pst DC3000(AvrRpt2)
Relative Value of mRNA(IUBQ10)
IAN7
IAN8
IAN9

Figure 2

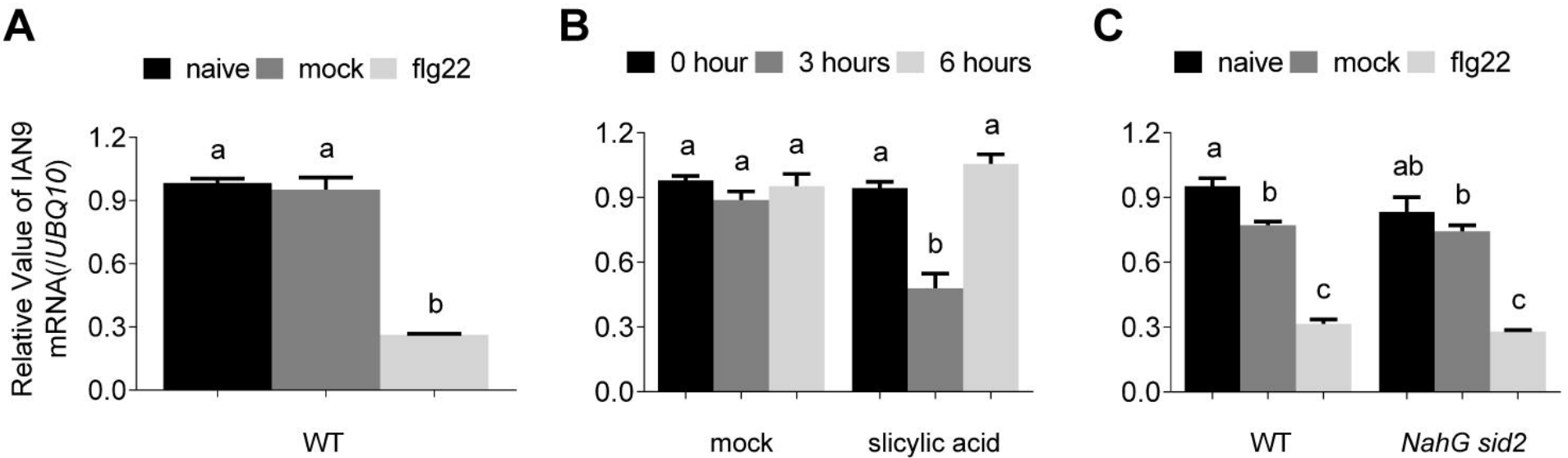
A
naive
mock
flg22
Relative Value of IAN9 mRNA(*IUBQ10*)
1.2
0.9
0.6
0.3
0.0
a
a
b
WT
B
0 hour
3 hours
6 hours
a
a
a
a
b
a
mock
slicylic acid
C
naive
mock
flg22
a
b
c
ab
b
c
WT
NahG sid2

Figure 3

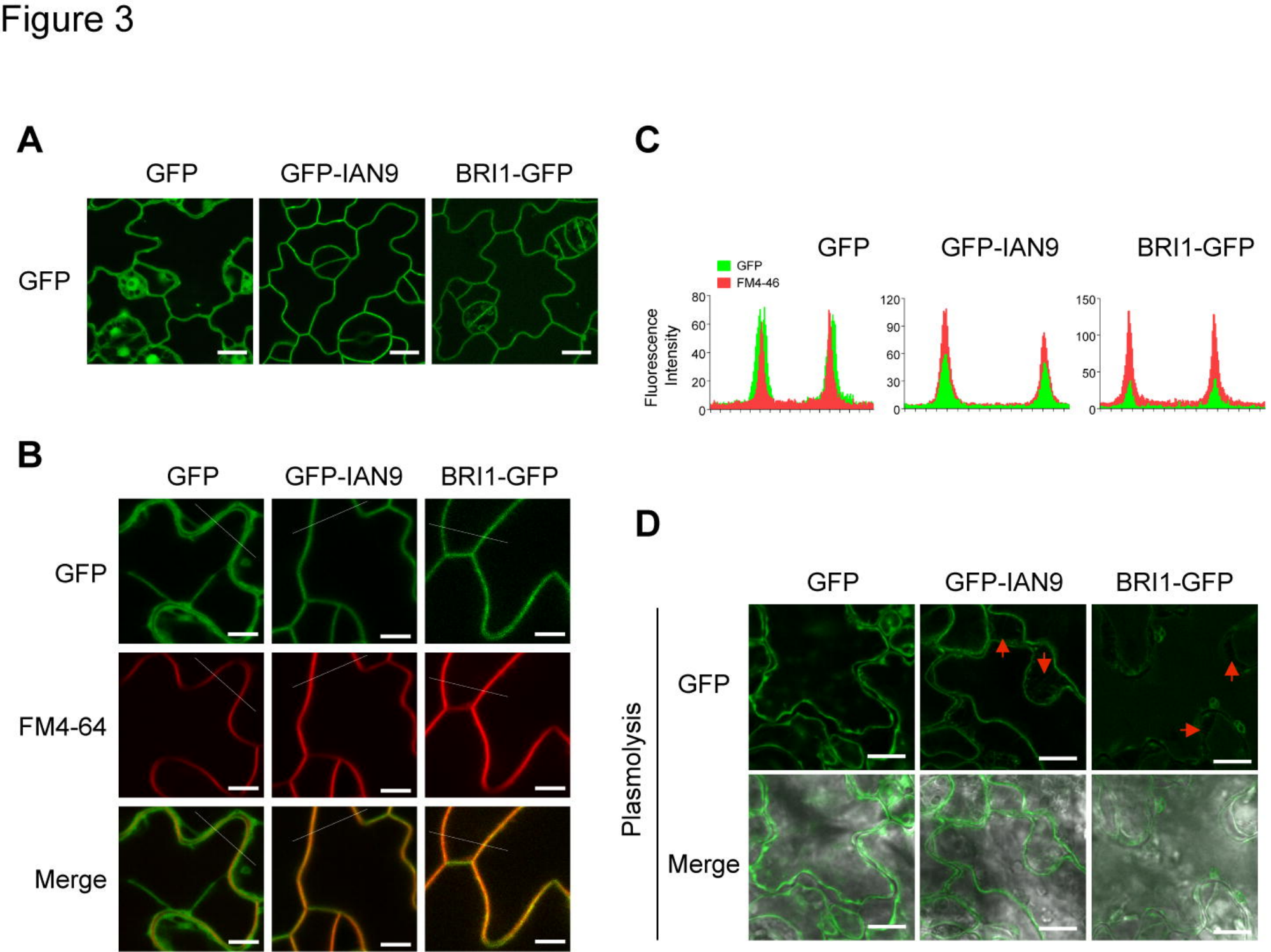
A
GFP
GFP-IAN9
BRI1-GFP
GFP
B
GFP
GFP-IAN9
BRI1-GFP
GFP
FM4-64
Merge
C
GFP
GFP-IAN9
BRI1-GFP
GFP
FM4-46
Fluorescence Intensity
80
60
40
20
0
120
90
60
30
0
150
100
50
0
D
GFP
GFP-IAN9
BRI1-GFP
Plasmolysis
GFP
Merge

Figure 4

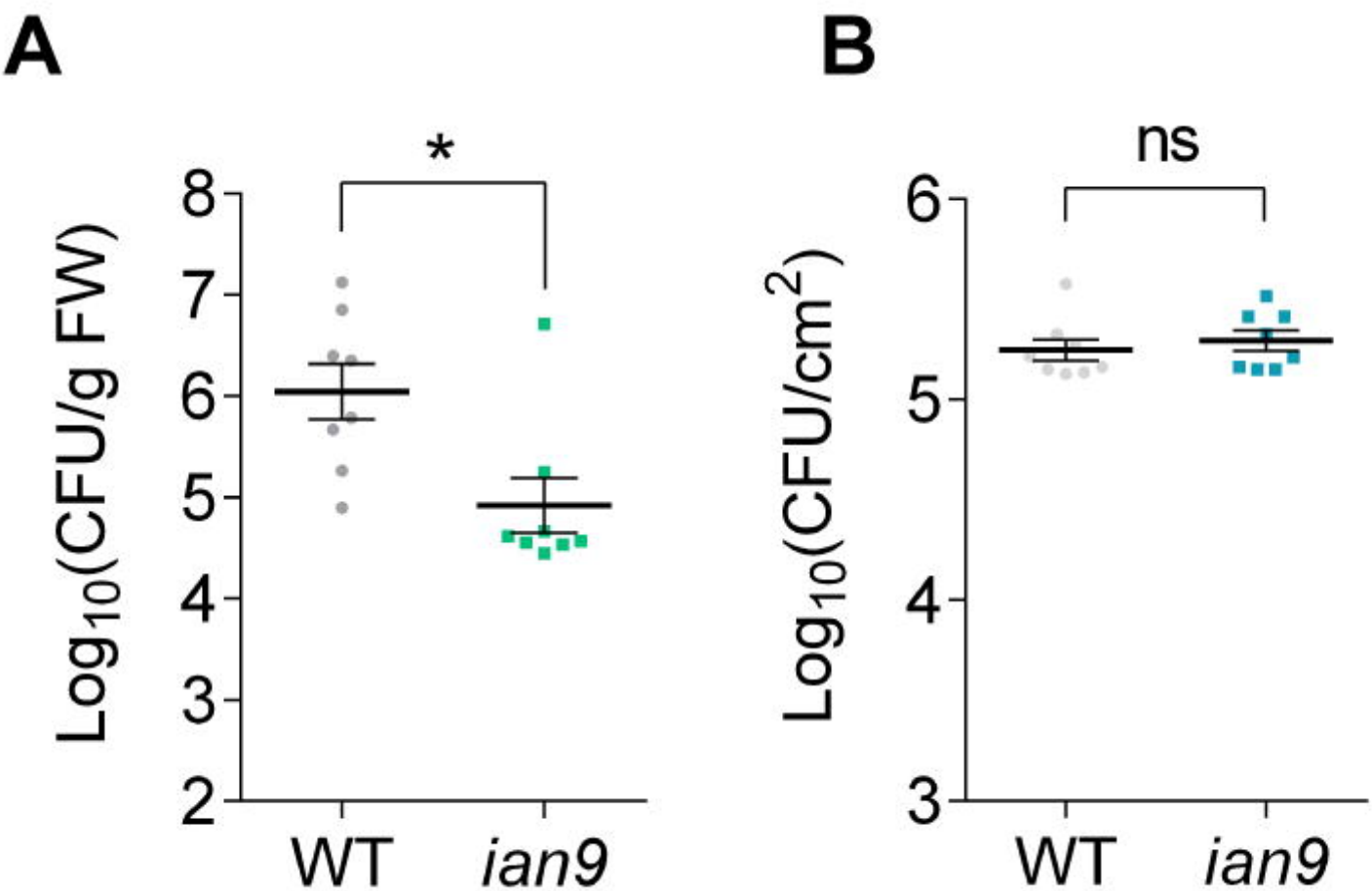

Figure 5

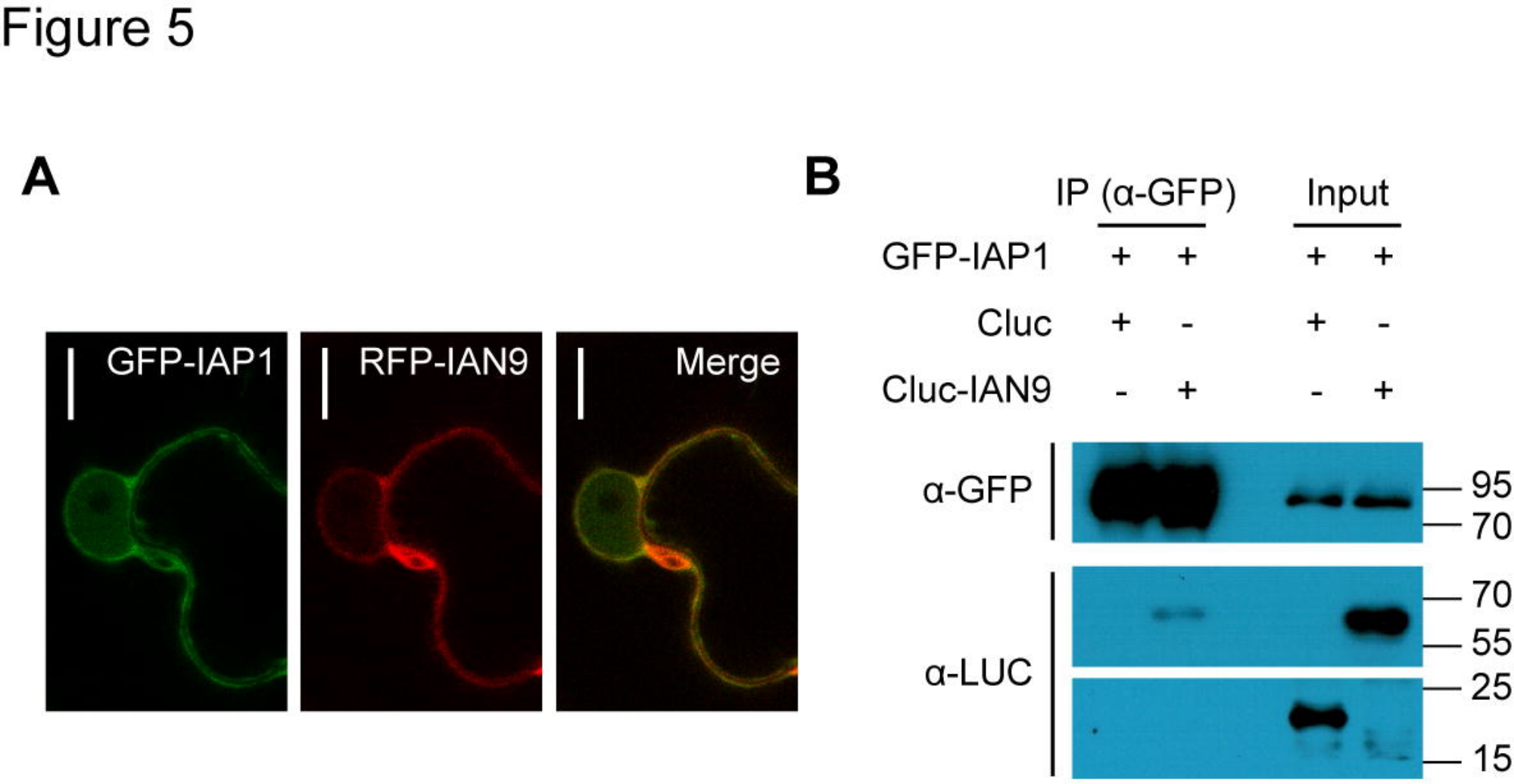
A
GFP-IAP1
RFP-IAN9
Merge
B
IP (α-GFP)
Input
GFP-IAP1 + + + +
Cluc + - + -
Cluc-IAN9 - + - +
α-GFP
α-LUC
95
70
70
55
25
15

Figure 6

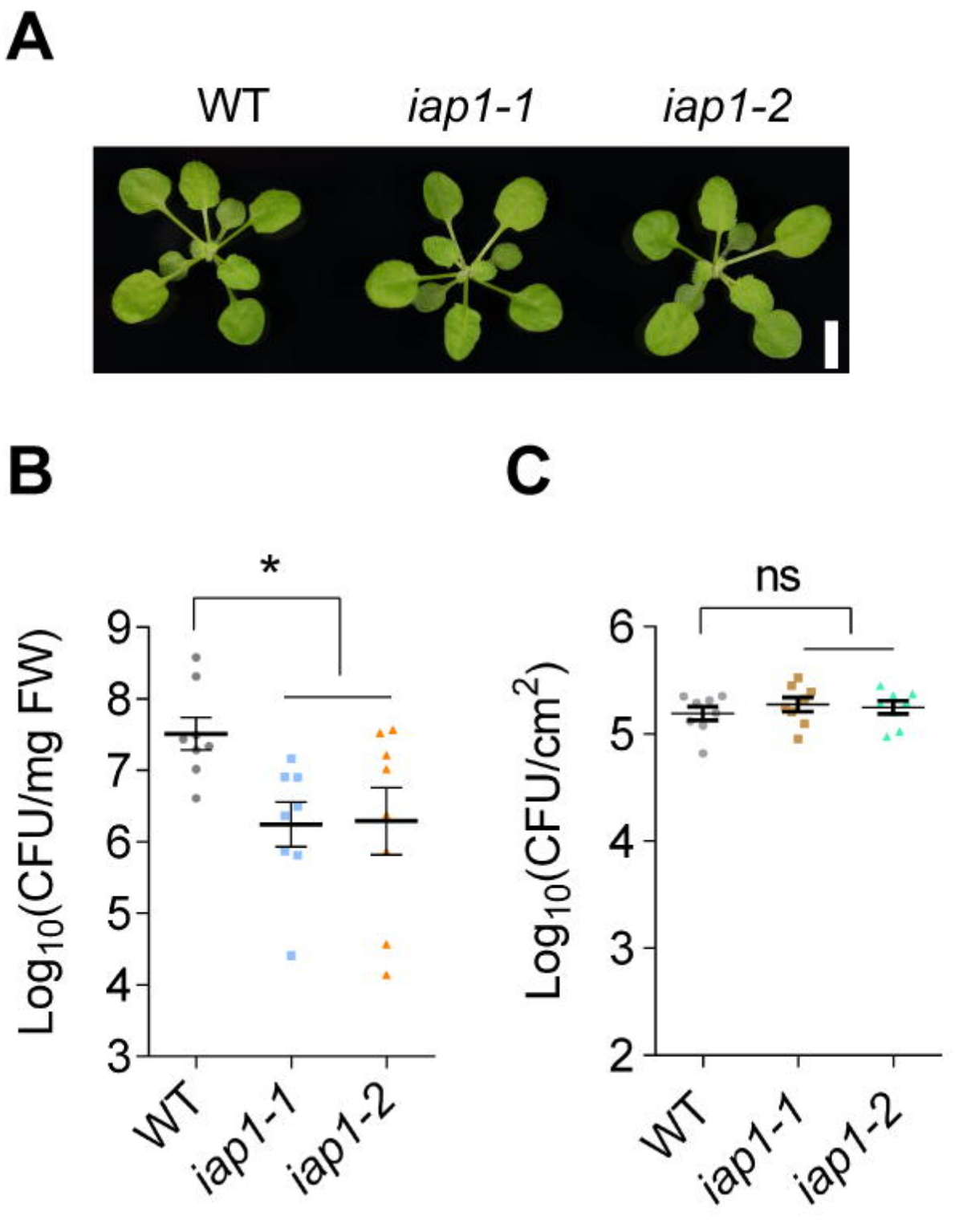
A
WT
iap1-1
iap1-2
B
*
Log10(CFU/mg FW)
9
8
7
6
5
4
3
WT
iap1-1
iap1-2
C
ns
Log10(CFU/cm2)
6
5
4
3
2
WT
iap1-1
iap1-2